ACS Catalysis

Research Article

pubs.acs.org/acscatalysis

Reversible Electron Storage in an All-Vanadium Photoelectrochemical Storage Cell: Synergy between Vanadium Redox and Hybrid Photocatalyst

Dong Liu, Wei Zi, Syed D. Sajjad, Chiajen Hsu, Yi Shen, Mingsheng Wei, and Fuqiang Liu*

Electrochemical Energy Laboratory, Department of Materials Science and Engineering, University of Texas at Arlington, Arlington, Texas 76019, United States

Supporting Information

ABSTRACT: Colossal solar energy conversion and storage studies using photoelectrochemical cells (PECs) have been undertaken in the past four decades; however, how to efficiently utilize solar energy despite the intermittent nature of sunlight still remains a challenge. In this paper, a WO_3/TiO_2 hybrid photoelectrode was coupled with our newly developed all-vanadium photoelectrochemical cell (PEC) with the aim of implementing photoelectrochemical solar energy conversion and storage. Zero-resistance ammetry (ZRA) and electrochemical impedance spectroscopy (EIS) were employed to study the photoelectrochemical response of this system in the conversion and storage of solar energy both under illumination and in the dark. The preliminary results proved the feasibility of this approach to store/release solar energy, even under dark conditions and showed that hydrogen tungsten bronze was responsible for the storage and release of photogenerated electrons from the semiconductor. The results also indicated an important synergy between electron storage and the all-vanadium electrolytes, which potentially offers great reversibility, high-capacity electron storage, and significant improvement in the photocurrent. To better understand the observed photoelectrochemical and electrochemical impedance behavior of our system, a model that unfolds the WO_3 electron storage mechanism and photogenerated charge carrier pathways in the all-vanadium PEC is proposed.

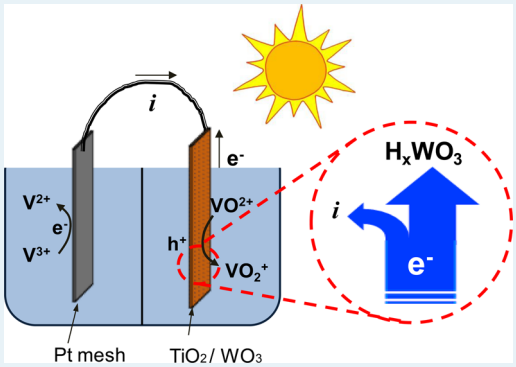

KEYWORDS: *vanadium redox, photoelectrochemical cell, WO_3/TiO_2, reversible electron storage, hydrogen tungsten bronze, solar energy*

1. INTRODUCTION

Photoelectrochemical hydrogen production by semiconductors and its subsequent use as an alternative to fossil fuels have been considered one of the most promising approaches to harness the unexhaustible energy from the sun and alleviate serious environmental problems for mankind. To split water, the thermodynamic requirements state that the conduction band and valence band edges of the semiconductor must straddle the threshold potential window of H_2 and O_2 evolution reactions unless an external bias is applied. To elaborate, the energy level of the conduction band edge of the semiconductor should be more negative than 0 V (H_2 evolution potential vs NHE at pH = 0), and the energy level of the valence band edge should be more positive than 1.23 V (O_2 evolution potential vs NHE at pH = 0) to incur photoelectrochemical water splitting.[1]

WO_3, an indirect bandgap semiconductor, along with its counterpart TiO_2, is one of the earliest photocatalysts that has received immense attention for photoelectrochemical water splitting.[2] Its relatively small bandgap energy (E_g = 2.6–2.8),[3,4] high resistance against photocorrosion, and excellent chemical stability over a wide range of pHs render it an even more suitable catalyst for photoelectrochemical water splitting, as compared with unabatedly studied TiO_2. However, the conduction band energy level of WO_3 is more positive than the standard reduction potential of water (0 V vs NHE); therefore, an external bias is often required to help drive the hydrogen evolution reaction.[5−7]

Despite such significant intrinsic drawback in terms of photoelctrochemical water splitting, WO_3 compared with other semiconductors has another distinctive characteristic, known as *electrochromism/photochromism* that enables its energy storage ability under certain conditions. Such an energy storage ability is realized through the formation of tungsten bronze by WO_3 reacting with electrons and certain cations in an electrochemical system under the circumstance of either an applied bias or solar illumination.

Although many studies[8−15] investigating the electrochromism/photochromism of WO_3 have been published in past two decades, those with respect to solar energy conversion and storage have just been pioneered by a group of Japanese

Received: December 16, 2014
Revised: March 10, 2015
Published: March 13, 2015

DOI: 10.1021/cs502024k
ACS Catal. 2015, 5, 2632−2639

researchers, such as Tatsuma and Fujishima in the 2000s. They developed a WO_3/TiO_2 hybrid energy storage system[16−18] in either electrolytes or gas phase and explored its applications in solar energy storage, steel corrosion protection, and as a bactericidal device. The latest work[4,19−22] using WO_3 for solar energy conversion and storage was investigated by Amal's lab at the University of New South Wales. They systematically studied WO_3 bulk thin films and flower-like nanostructured WO_3 synthesized by anodization in different electrolytes along with their ability in photoelectrochemical conversion and energy storage. They found that their WO_3 thin films can exhibit an energy storage ability under some generally perceived nonfavorable conditions: (i) a positive bias; (ii) the absence of a hole scavenger; (iii) under UV light illumination; and (iv) with no external source of electrons, if an appropriate electrolyte is employed. The generality between the Japanese researchers' work and that of Amal lies in the supporting electrolyte in their systems, which employed alkali cations, such as Li^+, Na^+, and K^+. These cations are well-known to react with WO_3 and electrons to form tungsten bronze, thus enabling WO_3 the ability to store and release energy, as reviewed by Whittingham[23] back in 1968.

In this work, we also intend to utilize the energy storage ability of WO_3 to explore the possibility of photoelectrochemical solar energy conversion and storage, especially in the case of intermittent sunlight. However, unlike our predecessors, no Li^+, Na^+, or K^+ cations were used in our system to realize the energy storage ability of WO_3. Instead, our newly developed in situ solar energy conversion and storage cell,[24] an all-vanadium photoelectrochemical cell (PEC) was studied along with a hybrid WO_3/TiO_2 system. The combined system incorporates the conventional PEC, a vanadium redox-flow battery (VRB), and a WO_3/TiO_2 hybrid photocatalyst. Such a system is expected to have all the merits inherent to WO_3; its energy storage ability under dark conditions; and VRB, a well commercialized energy storage system: fast electrochemical kinetics, high charge/discharge round-trip efficency (up to 90%), low capital cost, and minimal safety issues. The preliminary results showed the great potential of our system for photoelectrochemical solar energy conversion and storage despite the intermittent nature of sunlight, even with an unmodified WO_3/TiO_2 hybrid photocatalyst.

2. EXPERIMENTAL SECTION

2.1. Electrode Preparation. TiO_2 and WO_3/TiO_2 hybrid (various WO_3 loadings) photoelectrodes with an active area of 6.45 cm^2 were fabricated and used throughout the experiment. To fabricate the TiO_2 and hybrid electrodes, 1.00 g of Degussa P25 TiO_2 (VP Aeroperl by Evonik) and 2.50 g of α-terpineol (laboratory grade, Fisher Scientific, USA) were mixed under constant stirring at 80 °C for 1 h to obtain a uniform TiO_2 or hybrid slurry with the addition of tungstic acid (Alfa Aesar, USA). Then the slurry was deposited on a precut, square, fluorine-doped tin oxide (FTO) (Pilkington, USA) substrate using a doctor blade. The FTO substrate was prewashed with acetone (99.7%, Fisher Scientific, USA), methanol (99.8%, Fisher Scientific, USA), and deionized (DI) water before being blow-dried and then further dried in an oven at 120 °C for 1 h. The obtained coating was subsequently calcined with air flow at 500 °C for 90 min.

2.2. Electrolyte Preparation. Three types of electrolytes, 3 M H_2SO_4, 0.01 M vanadium(IV, VO^{2+}) in 3 M H_2SO_4, and 0.01 M vanadium(III, V^{3+}) in 3 M H_2SO_4, were used in the experiments. The first two electrolytes were prepared by dissolving H_2SO_4 (96.6%, J.T. Baker, USA) in DI water with or without vanadium(IV) sulfate oxide hydrate ($VOSO_4{\cdot}xH_2O$) (99.9%, Alfa Aesar, USA). The number of waters in the $VOSO_4{\cdot}xH_2O$ was determined by thermogravimetric analysis. The prepared vanadium(IV)−sulfuric acid solution appeared light blue. The 0.01 M vanadium(III) electrolyte was obtained by electrochemically reducing the prepared vanadium(IV)−H_2SO_4 solution in an electrolytic cell at a constant current density of 3 mA/cm^2 using a potentiostat (Princeton Applied Research, Parstat 2273) until the potential reached 1.6 V. During the reduction, the electrolyte was protected by N_2 to prevent oxidation of the vanadium(III) species. The obtained vanadium(III)−sulfuric acid solution appeared light green.

2.3. Characterization. The crystallographic information on all of the electrodes was determined by XRD (Siemens, 810-M340-32-C3000) at a scan rate 0.01° s^{-1} between 20° and 80° with a dwell time of 1 s. No impurity other than anatase phase and rutile phase TiO_2 and monoclinic WO_3 was discovered from the XRD spectra (Figure S1 in the Supporting Information). Scanning electron microscopy (Hitachi S-3000 N variable pressure SEM) was used to examine the microstructure of all electrodes. The obtained SEM images (Figure S2 in Supporting Information) clearly show small WO_3 clusters on TiO_2 particles and mud cracks at higher WO_3 loadings, which was in agreement with our previous findings.[25,26] Raman spectra were collected using a PerkinElmer DXR Raman microscope from 100 to 2000 cm^{-1}.

The photoelectrochemical property of all electrodes was studied in a two-chamber, three-electrode electrochemical cell, in which the photoelectrode served as the working electrode (WE) and a platinum mesh and Ag/AgCl electrode served as the counter electrode (CE) and reference electrodes (RE), respectively. Details of the experimental setup have been described in our previous work.[24,26] Tests using zero-resistance ammetry (ZRA) were conducted up to almost 4 h with either 3 M H_2SO_4 or 0.01 M vanadium in 3 M H_2SO_4 electrolyte under dark and AM1.5 conditions. In a typical experiment, 3 M H_2SO_4 solution or 0.01 M V(IV) in 3 M H_2SO_4 was used as the anolyte, and 3 M H_2SO_4 solution or 0.01 M V(III) in 3 M H_2SO_4 was used as the catholyte in two chambers of the photoelectrochemical cell, separated by a Nafion 117 membrane.

Solar irradiation was created using an ozone-free solar simulator system (Newport, USA) coupled with an AM1.5 global filter (Newport, USA) and calibrated using a standard photodiode (Newport, USA). The electrochemical impedance spectroscopy (EIS) measurements in this study were performed on the electrochemical cell using either a TiO_2 or a hybrid electrode (24 wt % WO_3) under dark/AM1.5 illumination conditions. All data were recorded at open-circuit voltage (OCV) over a frequency range from 10 mHz to 2 MHz with an amplitude of 10 mV.

3. RESULTS AND DISCUSSION

We previously demonstrated the ability of WO_3 as an electron reservoir to store solar energy in an all-vanadium photoelectrochemical cell.[25,26] Such energy storage ability of WO_3 is believed to be enabled through one or more of the following routes: (i) the presence of UV illumination and a hole scavenger, (ii) application of a negative bias, or (iii) use of an external source of electrons. However, our previous work focused only on revealing the photoelectrochemical behavior of

DOI: 10.1021/cs502024k
ACS Catal. 2015, 5, 2632−2639

WO_3 and WO_3/TiO_2 hybrid electrodes under light for a short period of time (up to 3 min) and, therefore, may not reflect the long-term behavior of the cell. In addition, it is unclear if the energy storage behavior of the system is reversible. To this end, a prolonged photoelectrochemical study (up to almost 4 h) was conducted in this work to investigate the overall cell performance in terms of electron storage using two distinct electrolytes.

Figure 1 depicts the photocurrent of different electrodes in 3 M H_2SO_4 electrolyte under alternate dark/illumination

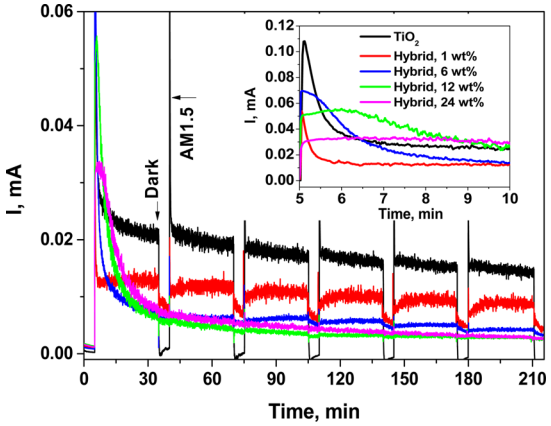

Figure 1. Photocurrent measurements of PECs with different electrodes in 3 M H_2SO_4 electrolytes under alternate dark/illumination conditions. The inset graph shows the photocurrent of different electrodes from 5 to 10 min under illumination.

conditions, and the inset graph magnifies the photoresponse from 5 to 10 min under illumination. Generally, all electrodes show a relatively small photocurrent under AM1.5 illumination, which is an indication of sluggish reaction kinetics of H_2 and O_2 evolution. Compared with the TiO_2 electrode, the hybrid electrodes show even inferior photocurrent within almost the entire test window, although it has been observed that increasing the loading of WO_3 in the hybrid electrodes resulted in a red shift of the absorption shoulder, which occurred near 450 nm.[25] However, the inset graph indicates a higher photocurrent for the hybrid electrode with 12 wt % of WO_3 than that of TiO_2 electrode during the first 5 min illumination, which is consistent with our previous findings.[26] In addition, the photocurrents produced by the hybrid electrodes appear to reach saturation/stabilization eventually when the fraction of WO_3 is no less than 6 wt %, despite illumination.

On the other hand, the hybrid electrodes give much more appreciable dark current (at least 1 order of magnitude higher) than TiO_2 electrode. Unlike the negligible dark current by TiO_2, the one by the hybrid electrodes remains almost without any decay through each dark period (5 min). These findings achieved in prolonged testing seem to contradict our previous results observed in short-time tests, but can be well explained through the reversible intercalation/deintercalation of electrons and H^+ ions into/out of WO_3 to form hydrogen tungsten bronze, H_xWO_3. This is clearly seen from the appearance of all hybrid electrodes (Figure 2) before and after the photoelectrochemical experiments. The deeply colored blue-black hydrogen tungsten bronze appeared on all hybrid electrodes after AM1.5 irradiation, except the one with 1 wt % WO_3.

This observation coincides strongly with the photocurrent profiles of all hybrid electrodes in Figure 1. When light was

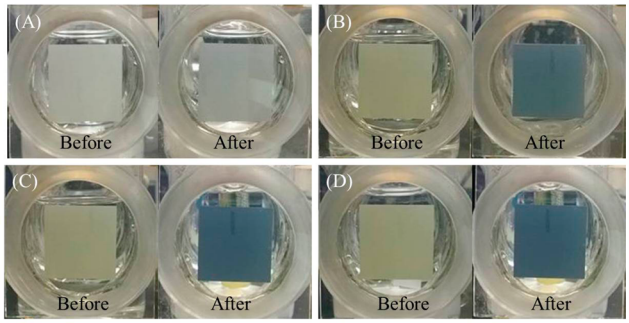

Figure 2. Appearance of hybrid WO_3/TiO_2 electrodes with WO_3 loadings of (A) 1 wt %, (B) 6 wt %, (C) 12 wt %, and (D) 24 wt % before and after ZRA experiment in 3 M H_2SO_4 electrolytes.

shed on the hybrid electrode, the photogenerated electrons, apart from recombining with holes at the semiconductor/liquid interface, had a higher tendency to react with WO_3 along with H^+ ions to form H_xWO_3. These H_xWO_3, scattered/distributed across the WO_3/TiO_2 matrix, are highly light-reflecting as a result of their metallic or quasimetallic nature[23,27,28] and are believed to act as a hurdle to electron transport, and thus, the photocurrent was reduced. This is especially clear when the photocurrent collected by the hybrid electrodes was examined. When the WO_3 content in the hybrid electrode is less dominant (e.g., 1 wt %), the photocurrent is only slightly mitigated, even under the long-term illumination test. However, the photocurrent was reduced to saturation/stabilization once the WO_3 loading was more than 1 wt %, regardless of the dark/illumination conditions. The noticeable dark currents from the hybrid electrodes are due to the released electrons from the decomposition reaction of hydrogen tungsten bronze. However, the reaction kinetics of such an electron release is believed to be very sluggish in pure acid, resulting in unchangeable dark currents for the hybrid electrodes, especially with high WO_3 loading.

Material characterization, such as Raman spectroscopy and XRD, was performed on the hybrid electrode (24 wt % WO_3) before and after ZRA experiments to confirm the formation of H_xWO_3. In the Raman spectra (Figure S3 in the Supporting Information), no peaks other than anatase TiO_2 and monoclinic WO_3 were observed. Five Raman active modes near 146, 197, 397, 515, and 633 cm^{-1} are assigned to characteristic vibration of anatase TiO_2.[26] The peaks near 270, 326, 713, and 806 cm^{-1} belong to characteristic vibration modes of monoclinic WO_3. XRD results (Figure S4 in Supporting Information), on the other hand, show structural changes of the hybrid electrode (24 wt % WO_3) after the ZRA tests. In Figure S4A, only peaks of anatase TiO_2 (JCPDS no. 21-1272), rutile TiO_2 (JCPDS no. 76-1940), and monoclinic WO_3 (JCPDS no. 83-0950) were found in the sample before the ZRA experiment. However, the crystal structure of WO_3 in the sample changed from monoclinic to cubic perovskite[29,30] after intercalation of hydrogen ions into the WO_3 lattice. The major structural change appears mostly on the three characteristic peaks of monoclinic WO_3 from 22.5° to 25° (Figure S4B), although other peaks remain the same after the formation of H_xWO_3. It is clear that not only do the three major WO_3 characteristic peaks disappear, but also two new peaks emerge in different positions. Dickens[29] reported that when hydrogen ions are inserted into a WO_3 lattice, all the corner-shared WO_6 octahedra are tilted relative to the orientation that is expected

DOI: 10.1021/cs502024k
ACS Catal. 2015, 5, 2632−2639

in a perovskite structure. Thus, it is believed that such a WO_6 octahedra tilt is responsible for the observed structural change of the hybrid electrode before and after the formation of H_xWO_3 in this study.

The photocurrents collected from the various electrodes in Figure 3 when the 0.01 M all-vanadium electrolytes were used

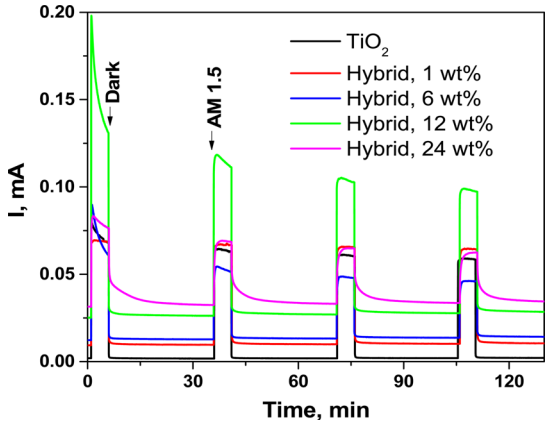

Figure 3. Photocurrent measurements of PECs with different electrodes in 0.01 M all-vanadium electrolytes under alternate dark/illumination conditions.

are significantly different from what is shown in Figure 1. The TiO_2 electrode demonstrated photoelectrochemical behavior distinctly different from the hybrid ones. All hybrid electrodes show a much higher photocurrent in an all-vanadium electrolyte compared with those in pure acid electrolyte. The improvement on the photocurrent is attributed to the mitigated charge carrier recombination and the fast reaction kinetics of the vanadium redox species. In addition, the amount of WO_3 in the hybrid electrode was discovered to play an important role affecting the photoelectrochemical behavior of the electrodes. When the WO_3 content in the hybrid electrode was either inadequate or abundant, the photocurrent was mitigated compared with that of TiO_2, and only a medium WO_3 loading (12 wt %) in the hybrid electrode gave the optimum photocurrent. This observation can be ascribed to the competition among vanadium redox reactions, the charge carrier recombination, and the tungsten bronze formation reaction at the semiconductor/liquid interface. When vanadium redox species were involved in the electrolyte, the photoelectrons preferentially participated in redox reactions, in addition to those in forming hydrogen tungsten bronze, as a result of the fast reaction kinetics of the vanadium species and the narrow band gap WO_3. It is deduced that the charge carrier recombination reaction dominates over the other reactions when WO_3 loading is insignificant; whereas WO_3 may induce charge trapping effects in the bulk[31] and form more hydrogen tungsten bronze when its loading is too high. An optimum amount of WO_3 in the hybrid electrodes serves as a mediator for effective charge carrier separation by minimizing the recombination losses with the assistance of vanadium redox species during illumination.

On the other hand, the ability of the hybrid electrodes to store photogenerated electrons compared with TiO_2 is conspicuously manifested in all-vanadium electrolytes by their dark current shown in Figure 3. Note that the test protocol shown in Figure 3 was slightly adjusted from that in Figure 1 to better exhibit the significant dark currents of the hybrid electrodes under illumination according to our preliminary experiments. In Figure 3, the hybrid electrodes were found to release electrons under dark conditions for prolonged periods of time, and the dark current was almost linearly proportional to the amount of WO_3 in the hybrid electrodes. The hybrid electrode with 24 wt % WO_3 exhibits substantial electron storage capacity under dark conditions(estimated to be 0.299 mAh/g or 1.078 C/g) in the form of a prolonged electron release up to 30 min (Figure S5 in the Supporting Information) with only 5 min of illumination. The released electrons from the hybrid electrodes under dark conditions are believed to be due to decomposition of hydrogen tungsten bronze formed during illumination, and they can be used to continue reducing the vanadium redox species, even in the dark. In other words, the photoelectrochemical cell could continually be charged, even under dark conditions, and this may open a new perspective for photoelectrochemical solar energy conversion and storage.

As exhibited in Figures 1 and 3, hydrogen tungsten bronze formed under illumination is believed to block the semiconductor/electrolyte interface and thus compromise the photocurrent. It is crucial then to study the charge transfer at the interface between the photoelectrode and electrolyte before, during, and after the illumination to understand its implication to photoelectrochemical kinetics. Electrochemical impedance spectroscopy is one of the most powerful techniques for investigating charge transfer processes in an electrochemical device. To this end, EIS measurement was conducted at the OCV of the cells on different photoelectrodes under dark/illumination conditions.

Figures 4 and 5 represent the Nyquist plots of the TiO_2 and hybrid (24 wt %) electrodes, respectively, in pure acid or 0.01 M all-vanadium electrolytes under dark and illumination conditions. As shown in Figures 4 and 5, TiO_2 and hybrid electrodes show distinct characteristics of impedance in two electrolytes, albeit their spectra are all composed of similar arcs/partial arcs. Generally, an arc in the Nyquist plot represents the existence of an electrochemical interface, and the appearance of plural arcs indicates different time constants of electrochemical interfaces for electron transport in the electrochemical system.

When only a 3 M H_2SO_4 electrolyte was used (Figure 4A), the high-frequency arc and an even bigger arc (only a portion) at low frequency, according to consensus in literature,[32,33] are believed to correspond to electron transport resistance and interfacial capacitance at the Pt/electrolyte and TiO_2/electrolyte interface, respectively. The dominantly large diameter of the low-frequency arc indicates huge charge transfer resistance and, thus, sluggish reaction kinetics,[34] regardless of illumination. This finding corroborates the observation in Figure 1, indicating water splitting by TiO_2 is intrinsically sluggish. Note that the diameter of the small arc at high frequency is independent of the dark/illumination conditions, proving that no change occurred on the Pt electrode itself. However, when vanadium redox species were involved in the electrolyte (Figure 4B) and new interfaces were created, a big difference was seen on impedance spectra compared with Figure 4A. One more arc with a much larger diameter emerged at midfrequency, and it represents the charge transfer resistance and interfacial capacitance at the TiO_2/vanadium(IV) redox interface. The new arc at midfrequency dominates much more in the whole impedance spectra than the electron transport at high frequency and Warburg diffusion resistance at low frequency.

DOI: 10.1021/cs502024k
ACS Catal. 2015, 5, 2632−2639

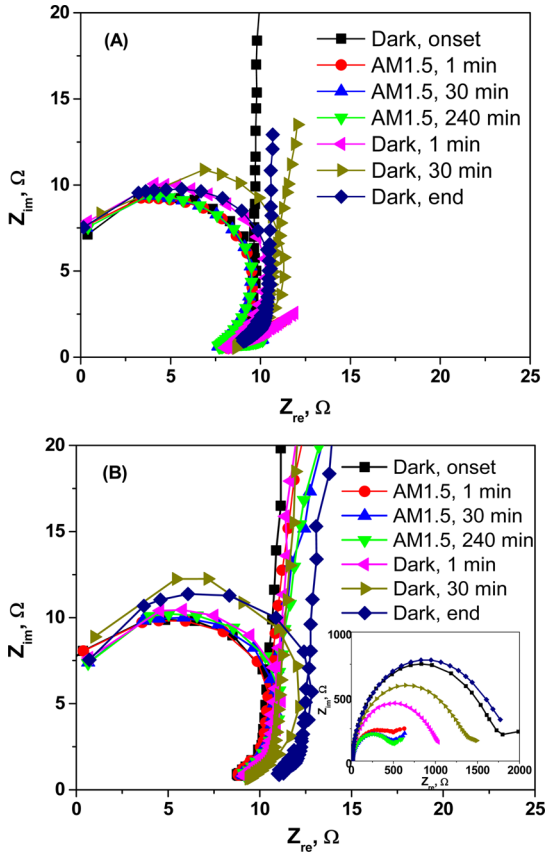

Figure 4. Nyquist impedance spectra of PECs in (A) 3 M H_2SO_4 electrolytes and (B) 0.01 M all-vanadium electrolytes with a TiO_2 photoelectrode. The inset graph in Figure 4B represents Nyquist plots of the cell under various conditions for all of the tested frequencies.

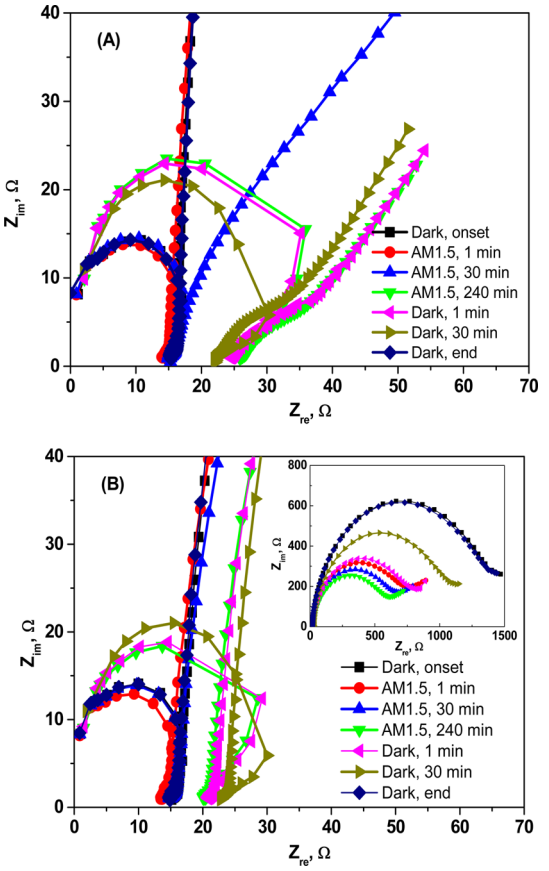

Figure 5. Nyquist impedance spectra of PECs in (A) 3 M H_2SO_4 electrolytes and (B) 0.01 M all-vanadium electrolytes with a hybrid (24 wt % WO_3) photoelectrode. The inset graph in Figure 5B represents Nyquist plots of the cell under various conditions for all of the tested frequencies.

Although not fully understood, this result indicates that vanadium redox plays a vital role at the TiO_2/vanadium(IV) redox and Pt/vanadium(III) redox interfaces in terms of charge transfer resistance and electron transport resistance.

In addition, the new interfaces created by vanadium redox species seem to have little influence on the electron transport resistance at the counter electrode because the resistance values (see the magnified inset graph in Figure 4B) are very similar to their counterparts in Figure 4A, regardless of the dark/illumination conditions. However, the charge transfer resistance with vanadium redox species was considerably reduced, up to 3 times, under AM1.5 illumination. This is due to facilitated electron generation and transport by fast reaction kinetics of the vanadium redox, which is in agreement with Figure 3. As indicated in our previous study,[26] the vanadium redox also shifts the dynamic balance between the charge carrier recombination and redox reaction toward the latter, which is verified in Figure 4B. The electron transport resistance (diameter of the midfrequency arc) after illumination for 1 min (red line) was greatly reduced and quickly reached stabilization in 30 min (blue line). The EIS spectra remained unchanged, even up to 4 h (green line). In addition, when the light was turned off, the electron transport resistance was promptly increased and reverted back to its original value as before the test. Comparison between Figure 4A and B clearly reveals the quick charge transfer at the semiconductor/electrolyte interface when vanadium redox species were employed.

Figure 5 depicts the Nyquist plots of the hybrid (24 wt % WO_3) electrode in the photoelectrochemical cell using two electrolytes. They have characteristic arcs/diffusion components that are similar to those of TiO_2 in Figure 4, but with some obvious differences. As suspected from Figure 1, hydrogen tungsten bronze formed under illumination by WO_3 reacting with photogenerated electrons and H^+ ions in the electrolyte is realized as a hurdle to electron transport at the semiconductor/electrolyte interface. Such speculation is confirmed from the impedance spectra shown in Figure 5. The electron transport resistance corresponding to the Pt/electrolyte interface (i.e., diameter of the high-frequency arc) in both electrolytes was nearly doubled under illumination, and this increase was strictly dependent on time, although the nature of the Pt/electrolyte interface at the counter electrode remained unchanged; however, the charge transfer kinetics might be impeded under illumination because the incoming electrons from the photoelectrode are blocked by the formation of H_xWO_3.

It is seen in Figure 5B that an increase in electron transport resistance, as a result of H_xWO_3 formation, appeared delayed in all-vanadium electrolytes. In addition, the electron transport resistance after long-term illumination (4 h) was ~5 Ω lower than that in 3 M H_2SO_4 electrolytes. Such results are consistent with the observed saturated photocurrent of the hybrid (24 wt % WO_3) electrode in Figure 1 and the electrode appearance change in Figures 2 and 6. It is believed that fast reactions of

DOI: 10.1021/cs502024k
ACS Catal. 2015, 5, 2632−2639

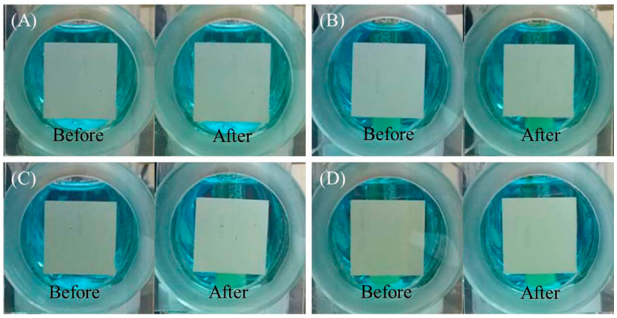

Figure 6. Appearance of hybrid WO_3/TiO_2 electrodes with WO_3 loadings of (A) 1 wt %, (B) 6 wt %, (C) 12 wt %, and (D) 24 wt % before and after ZRA experiment in 0.01 M all-vanadium electrolytes.

vanadium(IV) redox species at the photoelectrode surface, which quickly consume the photogenerated electrons, leave only a small fraction of those to participate in the formation of H_xWO_3. This significantly delays growth of H_xWO_3 on the photoelectrode and results in slow changes in both the high-frequency and midfrequency arcs in Figure 5B. The above analysis was confirmed by the unchanged electrode appearance (Figure 6) for different WO_3 loadings in 0.01 M all-vanadium electrolyte before and after the test.

To better understand the observed EIS spectra of the hybrid electrode in two electrolyte systems under different dark/illumination conditions, a model based upon the relevant electronic states of different components and standard electrochemical potential of different vanadium redox species is proposed in Figure 7. This model also helps further elucidate

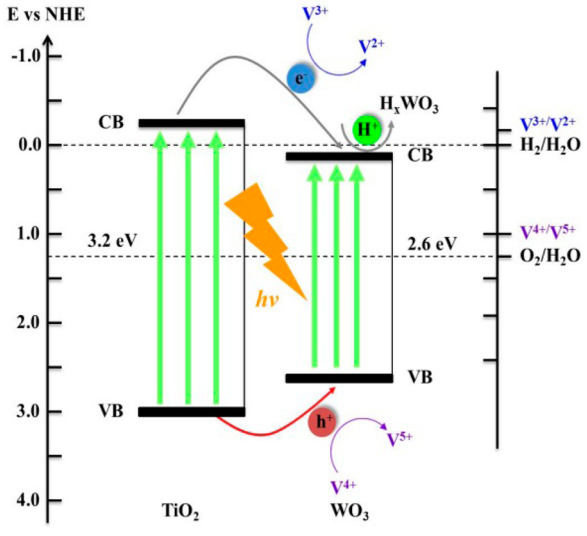

Figure 7. Schematic representation of proposed electron storage mechanism and charge transfer pathways for the hybrid WO_3/TiO_2 electrode in the all-vanadium photoelectrochemical storage cell.

the electron storage mechanism and charge transfer pathway for the hybrid electrode. In this model, to avoid unnecessary ambiguity, the bandgap energy of WO_3 is designated as 2.6 eV, and the conduction band (CB) edge is ~0.4 V more positive than that of TiO_2 in the electrochemical scale that is typically reported in the literature,[2,6,7,35−37] although controversy remains in the academic society that the bandgap energy of WO_3 spans from 2.6 to 3.3 eV. However, these values differ mainly in the position/maximum energy level of the valence band (VB) and, thus, shall have little impact on our discussion regarding the electron storage mechanism for the hybrid electrode and charge carrier transfer processes.

As illustrated in Figure 7, the photogenerated electrons and holes in TiO_2 need to travel "downhill" and "uphill" to the CB and VB of WO_3, respectively, because of their relative band positions. The more positive CB and more negative VB of WO_3 are deemed the driving forces for such charge carrier migration. During this process, different reaction scenarios emerge, depending on the electrolyte used. When pure acid was employed as the electrolyte, photogenerated holes from TiO_2 and WO_3 oxidize H_2O, resulting in O_2 evolution, and the photoelectrons react with WO_3 and H^+ ions to form hydrogen tungsten bronze. This is why the blue-black coloration appeared on the electrodes after illumination in pure acid electrolyte. Note that such photochromism highly depends on the amount of WO_3 that participates in the reaction and electron transfer kinetics. When WO_3 loading in the hybrid electrode is insignificant (e.g., 1 wt %), the photochromism is insignificant (Figure 2) because little difference was found after long-term illumination up to 4 h by examining the electrode appearance. However, the noticeable dark current observed after switching off the light clearly indicates the formation of hydrogen tungsten bronze and its slow decomposition to release electrons. As for the hybrid electrodes with higher WO_3 loading, blue-black coloration (Figure 2) was observed after the same test, and the photocurrent (Figure 1) during the test quickly reached saturation/stabilization, regardless of the dark/illumination conditions. These observations confirm that (i) hydrogen tungsten bronze is preferably formed out of hybrid electrodes under AM1.5 illumination; (ii) it renders as the barricade to prevent electron transfer; and (iii) the decomposition is very slow, as revealed in Fujishma's work.[10]

When vanadium redox species were involved in the electrolyte, photogenerated charge carriers had a distinct pathway at the semiconductor/liquid interface. Similar to the previous scenario, photogenerated holes from TiO_2 will still travel "uphill" to the WO_3 VB and join their counterparts there. Instead of evolving O_2, these holes are inclined to oxidize vanadium(IV) ions to vanadium(V) ions because of the more negative electrochemical potential and faster reaction kinetics of V^{4+}/V^{5+} redox,[25,26] as compared with oxygen evolution reaction. On the other hand, the photogenerated electrons from TiO_2 are speculated to mainly/completely react with vanadium(III) ions in the catholyte and reduce them to vanadium(II) ions when they travel "downhill" to the conduction band of WO_3 as a result of fast electrochemical kinetics of V^{3+}/V^{2+} redox. The remaining photogenerated electrons from TiO_2, if any, along with their counterparts in WO_3 will react with WO_3 to form hydrogen tungsten bronze. This process is reverted under dark conditions upon demand, releasing the stored electrons. This finding is confirmed by the prolonged dark current (Figure 3 and Figure S5) and EIS measurement (Figure 5B) as the resistance was increased after long-term illumination, which indicates the existence of hydrogen tungsten bronze.

Meanwhile, the fast reaction kinetics of the V^{3+}/V^{2+} redox is believed to prevent TiO_2 photoelectrons from recombination, thus providing a much higher photocurrent than what is exhibited in a pure acid electrolyte. In other words, the hybrid electrode is capable of revitalizing photocurrent in all-vanadium electrolytes under illumination and releasing electron energy stored in hydrogen tungsten bronze under dark conditions

DOI: 10.1021/cs502024k
ACS Catal. 2015, 5, 2632−2639

simultaneously. Note that the magnitude of the photocurrent revitalized and the electron energy released strongly depend on the amount of WO_3 in the hybrid electrode and redox reaction kinetics. Most importantly, the electron storage capability of the hybrid electrode when coupled with the all-vanadium electrolytes, in comparison with pure acid electrolytes, potentially offers great reversibility (Figure 6), long-term electron storage (up to 4 h in Figure 5), and significant improvement in the photocurrent (Figure 2). Because what has been demonstrated here in this work employed only unmodified semiconductors, it is envisioned that further improvement can be brought in by future optimization to enable practically meaningful continuous solar energy conversion and storage using advanced semiconductors in a tandem structure.

4. CONCLUSION

The energy storage ability of WO_3 was investigated using WO_3/TiO_2 hybrid photoelectrodes in an all-vanadium photoelectrochemical storage cell under either dark or illumination conditions. ZRA and EIS were used to probe the photoelectrochemical and electrochemical behavior of the cell with respect to photoelectrochemical solar energy conversion and storage. Results revealed mitigated photocurrent in pure acid electrolyte but enhanced photoresponse of the hybrid electrodes in all-vanadium electrolytes under long-term illumination. Without applying the bias, hydrogen tungsten bronze was formed in both pure acid and all-vanadium electrolytes, and this finding was corroborated by EIS results and material characterization results. In pure acid, the formed hydrogen tungsten bronze acts as a hurdle to prevent electron transport and thus mitigates the photocurrent, whereas all-vanadium electrolytes are beneficial to revitalize photocurrent of the hybrid electrodes under illumination and realize energy storage ability of WO_3 under dark. However, a complicated interplay was found to exist between the achieved photocurrent and the released dark current by using different WO_3 loadings in the hybrid photoelectrode. A model was then proposed to elaborate the observed experimental results and the charge carrier transfer pathways. The vanadium redox species, because of their fast electrochemical kinetics, not only enhance the photocurrents under illumination through mitigating formation of H_xWO_3, but also help release reversely stored electrons under dark.

■ ASSOCIATED CONTENT

Supporting Information

The following file is available free of charge on the ACS Publications website at DOI: 10.1021/cs502024k.

The crystallographic, morphological, and spectroscopic characterization results of all fabricated electrodes before and after electrochemical experiments (PDF)

■ AUTHOR INFORMATION

Corresponding Author

*Phone: +1-817-272-2704. Fax: 817-272-2538. E-mail: fuqiang@uta.edu.

Notes

The authors declare no competing financial interest.

■ ACKNOWLEDGMENTS

This work was financially supported by the National Science Foundation under Grant No. ECCS-1254915.

■ REFERENCES

(1) Gu, J.; Yan, Y.; Krizan, J. W.; Gibson, Q. D.; Detweiler, Z. M.; Cava, R. J.; Bocarsly, A. B. *J. Am. Chem. Soc.* **2014**, *136* (3), 830−833.
(2) Hodes, G.; Cahen, D.; Manassen, J. *Nature* **1976**, *260*, 312−313.
(3) Gratzel, M. *Nature* **2001**, *414*, 338−344.
(4) Zhu, T.; Chong, M. N.; Chan, E. S. *ChemSusChem* **2014**, *7*, 2974−2997.
(5) Janáky, C.; Rajeshwar, K.; de Tacconi, N. R.; Chanmanee, W.; Huda, M. N. *Catal. Today* **2013**, *199*, 53−64.
(6) Alexander, D. B., Augustynski, J. In *On Solar Hydrogen and Nanotechnology*; Vayssieres, L., Ed.; Wiley: Chichester, UK, 2010; pp 333−348.
(7) Khaselev, O.; Turner, J. A. *Science* **1998**, *280*, 425−427.
(8) Higashimoto, S.; Nobuya, K.; Mori, K.; Azuma, M. *Catal. Lett.* **2005**, *101*, 49−51.
(9) Higashimoto, S.; Shishido, T.; Ohno, Y.; Azuma, M.; Takahashi, M.; Anpo, M. *J. Electrochem. Soc.* **2007**, *154*, F48−F54.
(10) Tatsuma, T.; Saitoh, S.; Ohko, Y.; Fujishima, A. *Chem. Mater.* **2001**, *13*, 2838−2842.
(11) Ngaotrakanwiwat, P.; Saitoh, S.; Ohko, Y.; Tatsuma, T.; Fujishima, A. *J. Electrochem. Soc.* **2003**, *150*, A1405−A1407.
(12) Hauch, A.; Georg, A.; Krašovec, U. O.; Orel, B. *J. Electrochem. Soc.* **2002**, *149*, A1208−A1211.
(13) Zhao, D.; Chen, C.; Yu, C.; Ma, W.; Zhao, J. *J. Phys. Chem. C* **2009**, *113*, 13160−13165.
(14) Bedja, I.; Hotchandani, S.; Kamat, P. V. *J. Phys. Chem.* **1993**, *97*, 11064−11070.
(15) Takahashi, Y.; Tatsuma, T. *Electrochem. Commun.* **2008**, *10*, 1404−1407.
(16) Ngaotrakanwiwat, P.; Tatsuma, T.; Saitoh, S.; Ohko, Y.; Fujishima, A. *Phys. Chem. Chem. Phys.* **2003**, *5*, 3234−3237.
(17) Tatsuma, T.; Saitoh, S.; Ngaotrakanwiwat, P.; Ohko, Y.; Fujishima, A. *Langmuir* **2002**, *18*, 7777−7779.
(18) Ngaotrakanwiwat, P.; Tatsuma, T. *J. Electroanal. Chem.* **2004**, *573*, 263−269.
(19) Ng, C.; Ng, Y. H.; Iwase, A.; Amal, R. *Phys. Chem. Chem. Phys.* **2011**, *13*, 13421−13426.
(20) Ng, C.; Ye, C.; Ng, Y. H.; Amal, R. *Cryst. Growth Des.* **2010**, *10*, 3794−3801.
(21) Ng, C.; Ng, Y. H.; Iwase, A.; Amal, R. *ACS Appl. Mater. Interfaces* **2013**, *5*, 5269−5275.
(22) Ng, C.; Iwase, A.; Ng, Y. H.; Amal, R. *ChemSusChem* **2013**, *6*, 291−298.
(23) Dickens, P. G.; Whittingham, M. S. *Chem. Soc. Rev.* **1968**, *22*, 30−44.
(24) Wei, Z.; Liu, D.; Hsu, C.; Liu, F. *Electrochem. Commun.* **2014**, *45*, 79−82.
(25) Liu, D.; Liu, F.; Liu, J. *J. Power Sources* **2012**, *213*, 78−82.
(26) Liu, D.; Wei, Z.; Hsu, C.; Shen, Y.; Liu, F. *Electrochim. Acta* **2014**, *136*, 435−441.
(27) Yoon, D.; Manthiram, A. *Energy Environ. Sci.* **2014**, *7*, 3069−3076.
(28) Whittingham, M. S. *Solid State Ionics* **2004**, *168*, 255−263.
(29) Wiseman, P. J.; Dickens, P. G. *J. Solid State Chem.* **1973**, *6*, 374−377.
(30) Wang, L.; Yuan, L.; Wu, X.; Wu, J.; Hou, C.; Feng, S. *RSC Adv.* **2014**, *4*, 47670−47676.
(31) Paramasivam, I.; Nah, Y.-C.; Das, C.; Shrestha, N. K.; Schmuki, P. *Chem.—Eur. J.* **2010**, *16*, 8993−8997.
(32) Ahn, Y. R.; Park, C. R.; Jo, S. M.; Kim, D. Y. *Appl. Phys. Lett.* **2007**, *90*, 122106−1221063.
(33) Abayev, I.; Zaban, A.; Fabregat-Santiago, F.; Bisquert, J. *Phys. Status Solidi A* **2003**, *196*, R4−R6.
(34) Bard, J. A., Faulkner, R. L. *Electrochemical Methods: Fundamentals and Applications*; Wiley: New York, 2000; pp 383−387.
(35) González-Borrero, P. P.; Sato, F.; Medina, A. N.; Baesso, M. L.; Bento, A. C.; Baldissera, G.; Persson, C.; Niklasson, G. A.; Granqvist, C. G.; Ferreira da Silva, A. *Appl. Phys. Lett.* **2010**, *96*, 061909−0619093.

DOI: 10.1021/cs502024k
ACS Catal. 2015, 5, 2632−2639

(36) Yang, L.; Zhou, H.; Fan, T.; Zhang, D. *Phys. Chem. Chem. Phys.* **2014**, *16*, 6810−6826.
(37) Lu, X.; Xie, S.; Yang, H.; Tong, Y.; Ji, H. *Chem. Soc. Rev.* **2014**, *43*, 7581−7593.

DOI: 10.1021/cs502024k
ACS Catal. 2015, 5, 2632−2639